Available online at www.sciencedirect.com
ScienceDirect
Trans. Nonferrous Met. Soc. China 34(2024) 3569−3584
Transactions of Nonferrous Metals Society of China
www.tnmsc.cn

Fabrication of lightweight 3D interpenetrated NiTi@Mg composite with superior bending properties

Yu-jing LIU[1], Xiao-chun LIU[1], Kun-mao LI[2], Xiang WU[1], Sheng-feng ZHOU[2,3], Wei LI[2], Wen-cai ZHANG[4]

1. Institute of Metals, School of Materials Science and Engineering, Changsha University of Science & Technology, Changsha 410004, China;
2. Institute of Advanced Wear & Corrosion Resistance and Functional Materials, Jinan University, Guangzhou 510632, China;
3. State Key Laboratory of Mechanical Transmissions, Chongqing University, Chongqing 400044, China;
4. Department of Orthopedics, First Affiliated Hospital, Jinan University, Guangzhou 510632, China

Received 28 March 2023; accepted 7 November 2023

Abstract: A NiTi@Mg interpenetrating phase composite with high strength and lightweight was prepared by additive manufacturing (AM) and infiltration technology, and the interface bonding, three-point bending properties and cyclic compressive properties of NiTi@Mg composites were investigated. The results show that the metallurgically bonded interface is formed at the NiTi/Mg interfaces. The bending strength and compressive strength of the NiTi@Mg composite are 2.5 and 1.7 times higher than those of the NiTi scaffold, respectively. During the bending deformation process, a large number of dislocations are observed to accumulate in the soft Mg area at the interface. Furthermore, the finite element model showed that the stress accumulation area, where the bending crack is initiated, is located at the interface of NiTi and Mg. The strengthening mechanism of NiTi@Mg composites is attributed to the twinning strengthening of Mg and heterogeneous structure strengthening.

Key words: metal composites; NiTi@Mg; bending properties; finite element simulation; strengthening mechanism

1 Introduction

Composite materials have emerged as an important research topic in material science. They achieve an excellent combination of properties and functions by the synergistic contribution of each constituent phase [1]. In the majority of composites, load-bearing responsibility is assigned to a stiff and strong phase (hard phase), while load transfer between the hard phases and the guarantee of structural stability are facilitated by a weak matrix (soft phase) [1]. However, the hard phases are mostly isolated in these traditional designs, such as heterogeneous lamella-structured composites [2], fiber-reinforced composites [3], and particle-reinforced composites [4]. Notwithstanding these designs can be endowed with good performance in specific loading directions, their performance will be greatly reduced in a more complex multi-axis states due to the lack of continuous reinforcement. An example is that fiber-reinforced composites exhibit higher strength under unidirectional tensile loading. Therefore, a continuous reinforcement design is deemed important for the preparation of composites with integrated structural stability and avoiding the introduction of weak directions.

A new design scheme, the interpenetrating

Corresponding author: Xiao-chun LIU, Tel: +86-18512481029, E-mail: xcliu@csust.edu.cn;
Kun-mao LI, Tel: +86-15329766509, E-mail: likunmao123@163.com;
Sheng-feng ZHOU, Tel: +86-18526333769, E-mail: zhousf1228@163.com

DOI: 10.1016/S1003-6326(24)66626-4

phase composites, has attracted the attention of researchers in recent years [5,6]. These composites are composed of two phases with topological interconnection throughout the whole structure. It has been consistently demonstrated in several studies that interpenetrating phase composites allow each constituent phase to be interconnected, which makes the optimal contribution to the mechanical properties of composites and provides an exciting alternative to the traditional designs (e.g., discontinuously reinforced composites) [1,6,7]. As such, interesting combinations of properties and functions can be achieved by the synergy of the two phases. For instance, composite materials with a completely interconnected three-dimensional network structure exhibit high strength, toughness, and wear resistance [8,9]. The reason for this is the continuous and distorted distribution of crystal packets within the network structure, which effectively inhibits the crack propagation in three-dimensional space [8]. It should be pointed out that the majority of interpenetrating phase composites in these studies are prepared by traditional strategies, such as mechanical mixing [10,11], powder metallurgy [12], hot pressing molding [13,14], and grouting molding [15]. To our disappointment, traditional methods for preparing composites exhibit insufficient controllability of the structure, resulting in limited mechanical or functional properties [16,17].

Additive manufacturing (AM), as exemplified by selective laser melting (SLM), is a technology capable of accurately manufacture complex structures and individualized shapes, making it an ideal method for preparing porous metals [18]. This is particularly effective in producing porous metal scaffolds with pre-designed architectures, thereby providing opportunities for ideal structural design. However, selective laser melting molding is limited and hindered in the preparing composites. For instance, selective laser melting for metals is restricted to a single ingredient (although material system is composed of multiple components). The process becomes significantly complicated when multiple types of ingredients are involved [6]. To address the issues, the fabrication of interpenetrating NiTi@Mg composites is divided into two steps: (1) preparing porous NiTi scaffolds using the selective laser melting method, and (2) infiltrating the scaffolds with a Mg melt. NiTi and Mg are chosen as ingredients due to the fact that NiTi alloy has low elastic modulus, good shape memory effect, and superelasticity, which can be applied in biomedical implant devices, actuators, and energy-damping structures. Additionally, NiTi alloy can release strain energy through stress-induced martensitic transformation during deformation [18,19]. While Mg possesses high specific strength, stiffness, and good damping properties, making it ideal for applications involving mechanical energy dissipation, vibration damping, energy absorption, and noise reduction [5]. Moreover, during deformation, Mg twinning plays an important role in hindering dislocation movement, buffering microcrack growth, and preventing catastrophic fracture [20]. However, the interface situation of Mg and NiTi materials remains unclear, and the corresponding deformation mechanism of the interface is still a research gap. Therefore, it is necessary to further explore the toughness mechanism of composite structures to provide guidance for the design of composite structural materials with excellent mechanical properties and functions. The initiation and propagation of interface cracks can significantly impact the strength and elongation of composite structures. Consequently, understanding the bonding situation and deformation mechanism of the composite structure interface can aid in the development of interpenetrating phase composite materials with higher strength and ductility.

This study reports the infiltration of Mg into a 3D printed NiTi scaffold to obtain 3D interpenetrating phase heterostructures composite materials. The mechanical properties and fracture behavior of the heterostructures are analyzed through three-point bending experiments, cyclic loading experiments, and finite element simulations. Focused ion beam (FIB) and transmission electron microscope (TEM) techniques are utilized to reveal the formation and failure mechanism of the NiTi@Mg interpenetrating phase heterostructures interface, providing guidance for designing composite structural materials with superior mechanical properties and novel functionalities.

2 Experimental

2.1 Fabrication of composite

This work employed two distinct metallic

materials: nickel-titanium (NiTi) powder and pure magnesium (Mg) powder. Spherical NiTi powder, with an average particle size of 35 μm, was utilized to fabricate scaffolds through selective laser melting (SLM) technique. NiTi scaffolds, comprising 10 × 10 × 30 arrays (with each cell size of 3.3 mm × 3.3 mm × 3.3 mm), were created using a Bolite SLM S210 machine (Bolite, China). The laser beam diameter during the SLM printing process was set to be 75 μm, and the layer thickness of the powders was 50 μm. The printing process was performed at a laser power of 200 W, and the scanning speed was set to be 1000 mm/s. This SLM process facilitated the fabrication of controlled NiTi reinforcement structures in interpenetrating phase composites. Subsequently, the Mg melt was infiltrated into the scaffold using a high-pressure chamber. Specifically, the NiTi scaffold and Mg were placed in the same crucible and maintained at 800 °C in a resistance furnace (OTF−1200X Kejnig, China) at a pressure of 10 MPa for 30 min, followed by cooling with the furnace. The heating process was conducted under the protection of an argon atmosphere, thereby enabling the preparation of NiTi@Mg inter-penetrating phase heterostructure composites while avoiding Mg oxidation. Figure 1 illustrates the detailed manufacturing process diagram of NiTi@Mg interpenetrating phase composites.

2.2 Mechanical properties test

A WDW-50 (Shanghai Bairuo, China) multifunctional mechanical testing machine was employed to conduct three-point bending and cyclic loading/unloading tests at ambient temperature. The dimensions of the three-point bending specimen were 30 mm × 10 mm × 10 mm, and the dimensions of the cyclic loading/unloading specimen were 10 mm × 10 mm × 10 mm. The three-point bending test was carried out at a strain rate of 0.5 mm/min. The cyclic compression samples were subjected to 10 loading/unloading cycles with a 2% strain increment. To ensure data reproducibility, at least three independent tensile samples were tested for each condition. The fracture morphologies were examined by scanning electron microscopy (SEM) and TEM. The hardness distribution at the NiTi/Mg interface was measured by the Lab Testing Tech THV-1D Vickers micro-hardness tester. The indentation load was set at 0.49 N with a residence time of 15 s. Randomly selected samples were tested at no less than five distinct positions, and the average value was recorded.

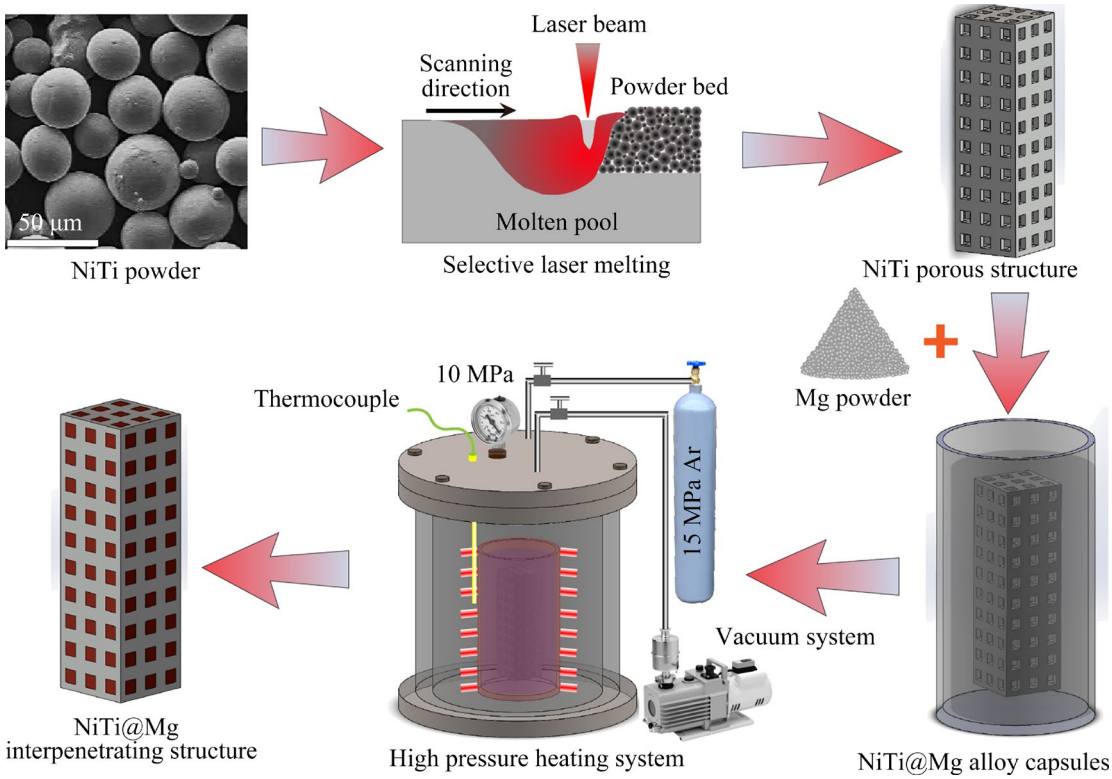

Fig. 1 Schematic illustration of fabrication process of NiTi@Mg interpenetrating phase composites, including preparation of NiTi metal stents by selective laser melting, and subsequent infiltration of scaffold with Mg melt

2.3 Structural characterization

The morphology of the NiTi scaffold and the NiTi@Mg interpenetrating phase structure, as well as the microstructure of fractured samples, were analyzed via SEM (JEOL JMS−7900F). SEM samples were prepared by mechanically grinding with 400−5000 mesh silicon carbide sandpaper, followed by polishing with colloidal Al_2O_3. The microstructure and energy dispersive spectroscopy (EDS) at the interface of the NiTi@Mg composite structure was examined using TEM (FEI Talos F200X) at 200 kV. TEM samples at the NiTi/Mg interface were prepared using the focused ion beam (FIB) method with a voltage of 30 kV (Thermoscientific Scions2). The observation areas included the NiTi/Mg interface before and after compression, respectively. Geometric phase analysis (GPA) was computed using custom GPA plugins in Gatan Digital Micrograph (DM) software.

2.4 Finite element modelling

The geometric models and dimensions of the three-point bending and compression tests were identical to those described in Section 2.2. Finite element simulations were conducted using commercial software, Abaqus 2021/CAE. The geometry of the three-point bending simulation loading system consisted of a loading probe, NiTi@Mg composite structure, and two rigid fixed supports. The loading rate of 0.5 mm/min was selected to match the experimental conditions. The compression simulation involved loading on volume elements of the NiTi@Mg composite material, with compression applied along the *y*-axis at a rate of 0.5 mm/min. Both the top and bottom anvils were approximated as rigid bodies with very high elastic moduli during numerical simulation. Additionally, the loading probe geometry during the simulation was modelled as a 3D−deformable−shell−planar structure.

3 Results

3.1 Microstructure and interfacial characteristics

Figure 2 displays the SEM images of the Ni scaffold and the NiTi@Mg interpenetrating structure, along with the hardness distribution at the NiTi/Mg interface. As can be observed in Fig. 2(a), the NiTi sample exhibits a cubic unit cell structure, where each unit cell has a size of 3.3 mm × 3.3 mm × 3.3 mm. Additionally, a large amount of splashed powder was observed in the porous NiTi scaffold, which increased the surface area of the scaffold and provided favorable conditions for the subsequent combination of NiTi and Mg [6]. The macro morphology of the NiTi@Mg interpenetrating structure formed by infiltrating Mg into porous NiTi scaffolds is shown in Fig. 2(b). The light-dark contrast areas represent the scaffold (NiTi) and the filler (Mg), respectively. Notably, no obvious defects are observed in either region of light-dark contrast, which verifies that thermal infiltration can prepare dense NiTi@Mg interpenetrating structures. The volume fractions of the filler and scaffold are approximately 50% each, which effectively prevents strain localization of the Mg fillers [15]. Moreover, no apparent macroscopic cracks and pores are found at the interface of the composites, indicating that the Mg fillers and NiTi scaffolds were effectively bonded.

Figure 2(c) shows the Vickers micro-hardness

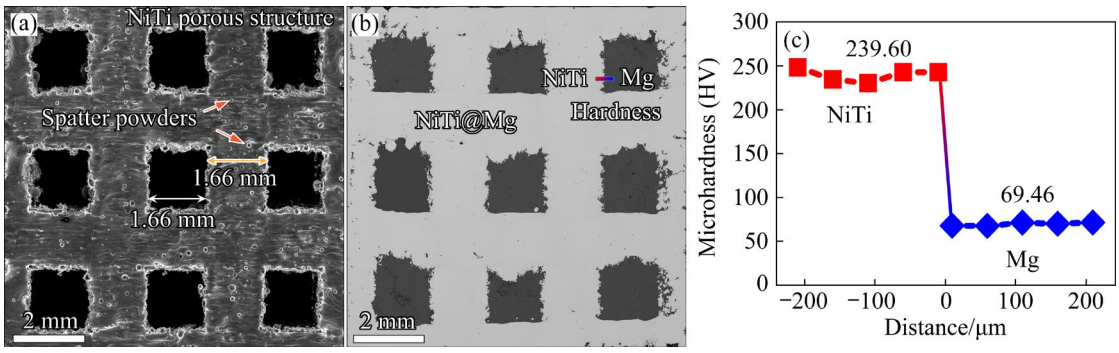

Fig. 2 (a) SEM images of SLM porous NiTi scaffolds; (b) SEM images of NiTi@Mg interpenetrating structure; (c) Vickers hardness of NiTi scaffold region and Mg filler region in (b) (Metallurgical bonding between hard phase NiTi scaffold and soft phase Mg filler)

of the scaffold (NiTi) and filler (Mg) of the NiTi@Mg composite. It can be observed that the micro-hardness of the Mg filler region (HV 69.46) is significantly lower than that of the scaffold region (HV 239.60). To a certain extent, this indicates that the deformation resistance of the filling area is smaller than that of the scaffold area. This matching of soft and hard regions can more effectively resist deformation [21].

To verify the bonding between NiTi scaffolds and the Mg fillers at the microscale, FIB was used to prepare TEM samples at the interface. The microstructure and composition distribution at the NiTi/Mg interface were measured by TEM and the results are shown in Fig. 3. It is found that there are significant differences in the microstructure between filler (Mg) and scaffolds (NiTi) at the interface, and the coarse grains and fine grains are identified as hexagonal close-packed (hcp) Mg and body-centered cubic (bcc) NiTi, respectively, by

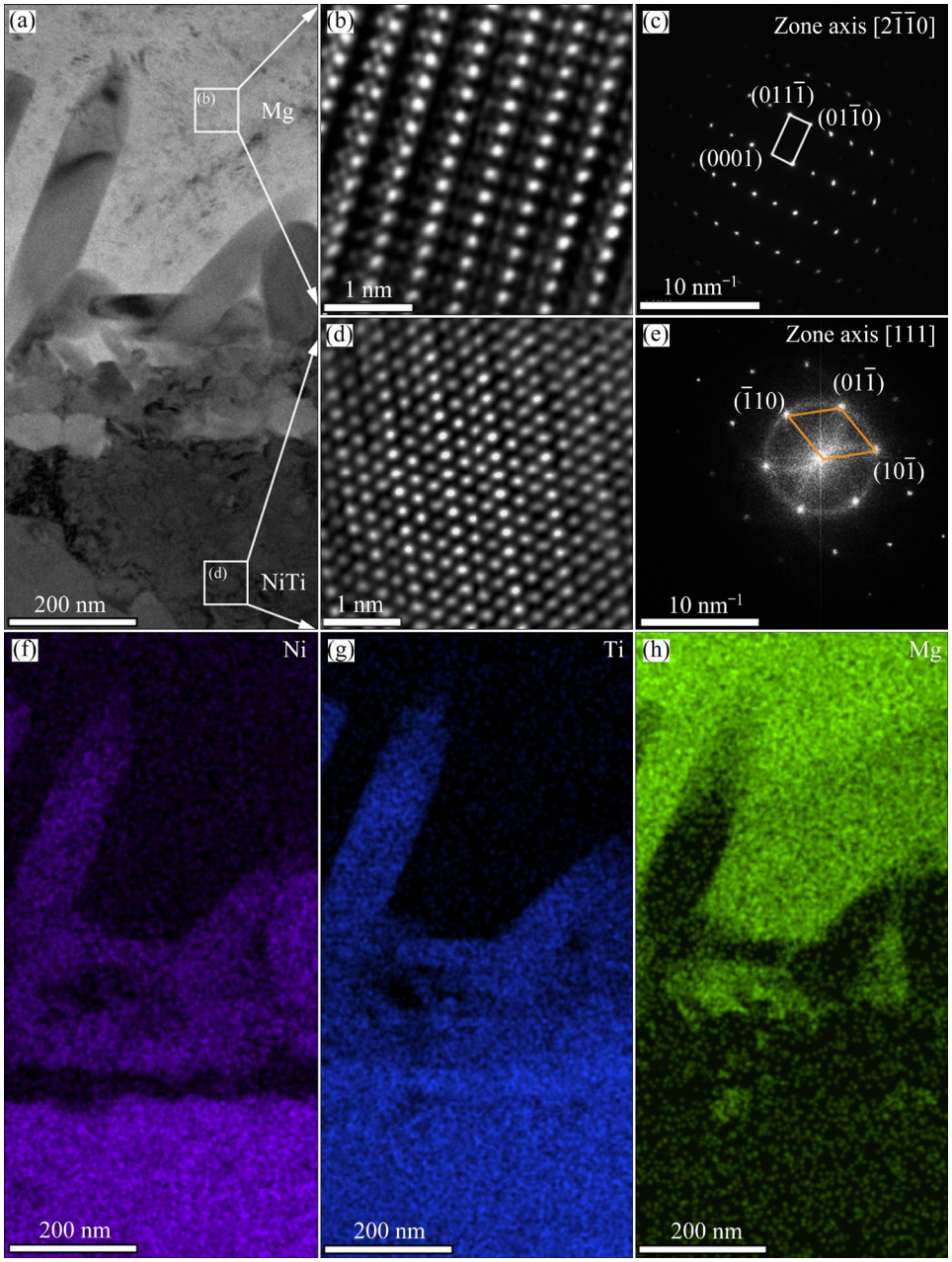

Fig. 3 TEM images for interface of NiTi@Mg sample: (a) Bright-field image; (b, c) [$2\bar{1}\bar{1}0$] zone axis high resolution transmission electron microscope (HRTEM) and selected-area electron diffraction (SAED) pattern of Mg filler in (a); (d, e) [111] zone axis HRTEM and SAED pattern of NiTi in (a); (f–h) STEM-EDS mapping images of interface region between NiTi scaffolds and Mg filler (The distribution spectra of Ni, Ti and Mg elements in the area are shown in (f), (g) and (h) respectively)

high resolution transmission electron microscopy (HRTEM) and selected area electron diffraction (SAED), as shown in Figs. 3(b, c) and (d, e). In fact, no visible microcracks were found at the NiTi/Mg interface, and the well-bonded microscopic interface is demonstrated in the TEM brightfield image (Fig. 3(a)). In addition, dendritic laths with a width of ~100 nm are precipitated at the interface of Mg and NiTi. These laths have a similar effect to the macroscopic sputtered powder (see Fig. 2(b)), i.e., increasing the roughness between the scaffold and filler, which provides an ideal condition for interface strengthening [6]. Figures 3(f−h) show the elemental mapping of Ni, Ti, and Mg, respectively. Elemental Ni and Ti are found both in the scaffold and filler area, which is attributed to the diffusion of Ni and Ti during the infiltration of the Mg into the scaffold. In addition, a small amount of Mg is also observed in the NiTi scaffolds. These results indicate that the interpenetrating NiTi@Mg specimens with metallurgical bonding interfaces are successfully prepared by SLM and infiltration, which will affect the mechanical properties of the scaffolds to some extent [5].

3.2 Mechanical properties

To assess the mechanical properties of the composites, three-point bending and cyclic loading compression experiments are conducted on the NiTi scaffolds and NiTi@Mg interpenetrating phase composites. The typical load−displacement curves are presented in Fig. 4(a). The three-point bending tests exhibit an initial linear increase in load−displacement curves, which indicates elastic deformation behavior.

After reaching the yield point of NiTi scaffolds and NiTi@Mg interpenetrating phase composites, the load and displacement continue to increase linearly. However, the load of the NiTi@Mg interpenetrating phase composite increases more prominently with displacement due to the hardening behavior of the interpenetrating phase composite after yielding [22]. The fracture resistance of both the NiTi scaffolds and the NiTi@Mg interpenetrating phase composites drops rapidly when the force reaches the peak load, and the samples deform severely until fracture occurs. Additionally, the bending strength and fracture absorption energy of the samples are demonstrated in Fig. 4(b). The NiTi scaffold exhibits a bending strength of 170 MPa, while the NiTi@Mg interpenetrating phase composite exhibits a bending strength of 432 MPa. The fracture absorption energies of the scaffold and interpenetrating phase composite are 16.49 and 41.33 J/mm^2, respectively. This result indicates that the NiTi@Mg interpenetrating phase composites possess much higher bending strength and energy absorption ability during the fracture process. Generally, this phenomenon can be attributed to the back stress generated by the filler [16,21,23]. During the three-point bending test, three characteristics can be observed in almost all materials: (1) Deformation initially occurs on the top surface in contact with the load, and the sample's cross-section may become elliptical, (2) The compressed part bends as the load increases continuously, and localized wrinkling occurs where the top surfaces meet and persist until failure, and (3) The material's ability to withstand load decreases rapidly when the curve reaches the peak load and exceeds the peak load displacement, indicating that the bottom of the material is broken [24].

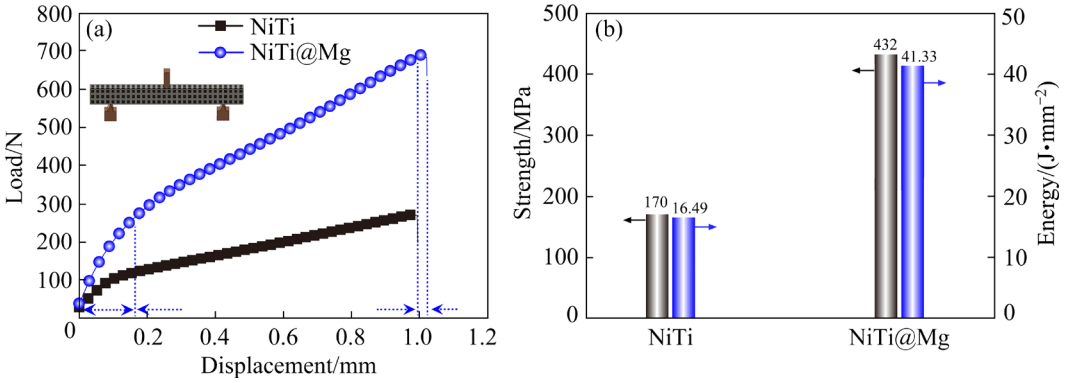

Fig. 4 (a) Typical load−displacement curves of NiTi scaffolds and NiTi@Mg interpenetrating phase composites; (b) Bending strength and fracture energy of NiTi scaffolds and NiTi@Mg interpenetrating phase composites (Compared with NiTi scaffold, NiTi@Mg interpenetrating phase composites have higher peak load and absorption energy)

Figure 5(a) depicts the stress−strain curves of NiTi scaffolds and NiTi@Mg interpenetrating phase composites under cyclic loading, and a similar trend is observed in ten-cycle compression tests of scaffolds and composites. The detectable circumscribed region in the stress−strain hysteresis loop indicates the presence of a hysteresis effect, which is more pronounced at higher strains. Under low strain compressive loads, the hysteresis loop is small, but it increases with strain. NiTi scaffolds exhibit a lower hysteresis effect than NiTi@Mg interpenetrating phase composites, as demonstrated in Fig. 5(b). These findings suggest that the hysteresis effect becomes more prominent as the applied strain increases, enabling additional dissipation of mechanical energy under cyclic loading/unloading conditions, in addition to dissipation through plasticity or damage [5].

To gain a deeper understanding of the deformation process of the interpenetrating phase composites, the characteristic energies, namely $E_{consumed}$ (irreversible deformation of mechanical energy consumption), $E_{disipated}$ (energy dissipated by viscoelasticity), and $E_{elastic}$ (energy of elastic recovery), are calculated for each loading cycle curve shown in Fig. 5(c). As illustrated in Fig. 5(d), the $E_{elastic}$ and $E_{dissipated}$ values of NiTi scaffolds and NiTi@Mg interpenetrating phase composites exhibit similar changes, reaching a steady state. However, after ten loading−unloading cycles, the $E_{elastic}$ and $E_{dissipated}$ values for NiTi@Mg interpenetrating phase composites are significantly higher than those for NiTi scaffolds, and their growth rate is also greater. A high $E_{elastic}$ is generally associated with high dissipation energy [5,22,25]. It should be noted, however, that the $E_{consumed}$ of NiTi@Mg interpenetrating phase composites is higher than that of NiTi scaffolds in the early stage, but after ten cycles of loading−unloading, their values become almost equal, implying that the Mg matrix can coordinate deformation during the plastic deformation stage [5].

3.3 Fracture morphology

Figure 6 presents the SEM fracture morphologies of NiTi scaffolds and NiTi@Mg interpenetrating

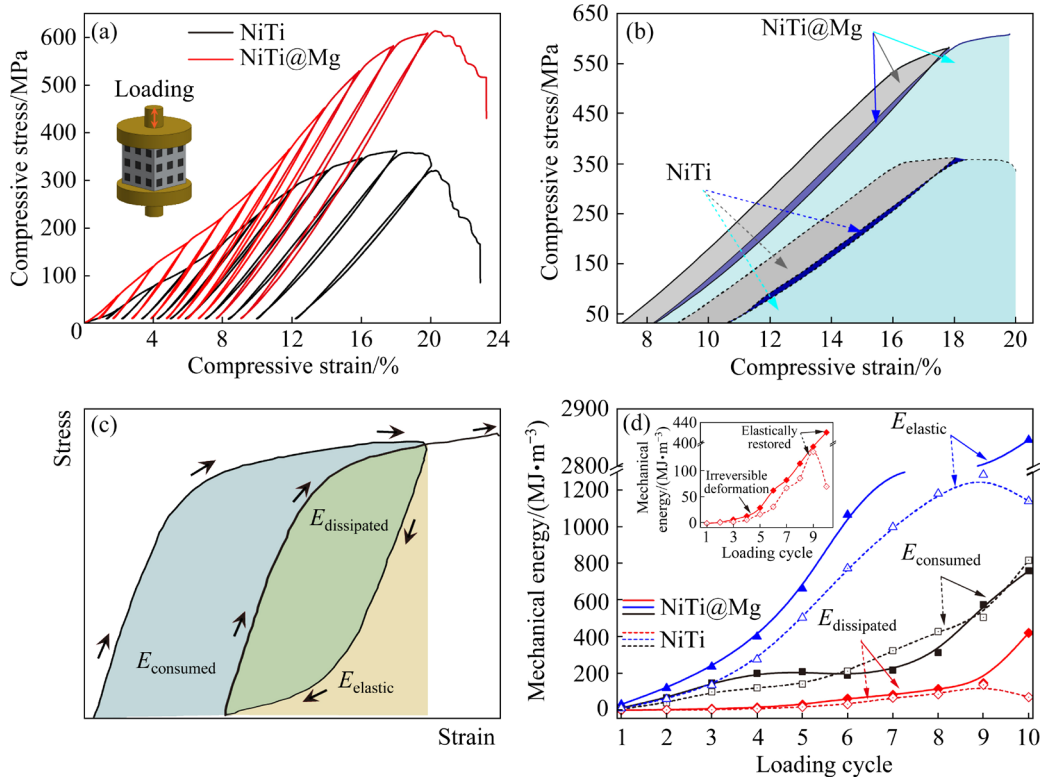

Fig. 5 Cyclic loading−unloading stress−strain curves of NiTi scaffolds and NiTi@Mg interpenetrating phase composites compressed to different strains: (a) Loading−unloading stress−strain curves compressed to different strains of 2%, 4%, 6%, 8%, 10%, 12%, 14%, 16%, 18% and 20%; (b) Stress−strain curves of composite at the 10th deformation; (c) Schematic diagram of mechanical energies distribution; (d) Variations of mechanical energy with loading cycle during cyclic loading−unloading process

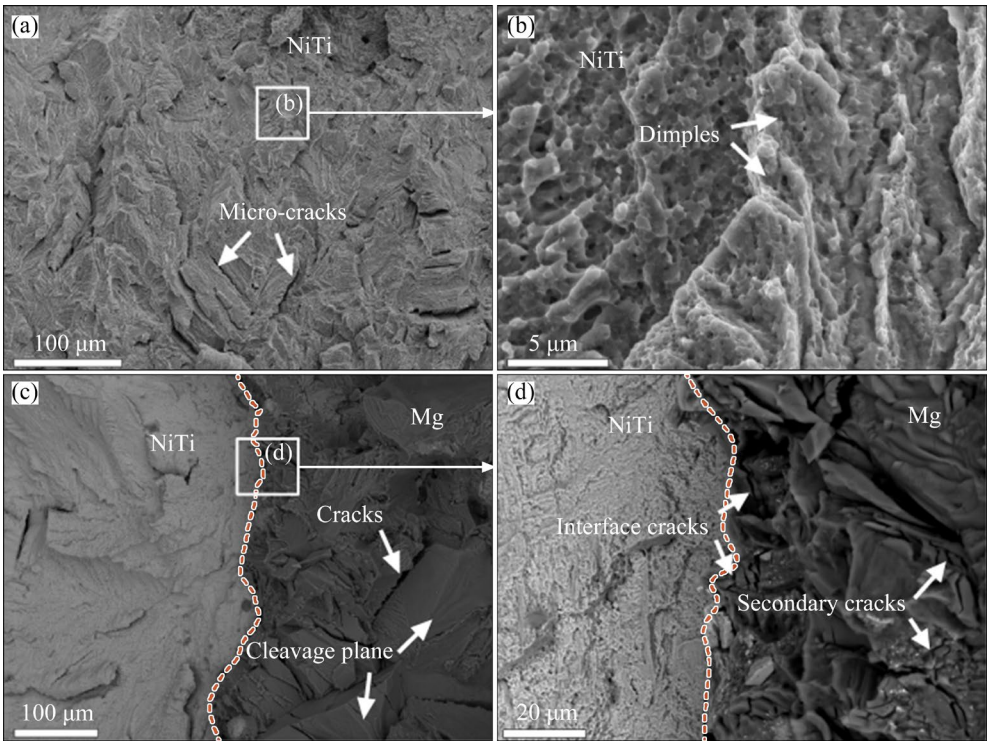

Fig. 6 SEM images of fracture surface morphology of NiTi scaffolds and NiTi@Mg interpenetrating phase composites: (a) Fracture surface of porous NiTi scaffolds; (b) Zoom-in image of boxed area in (a); (c) Fracture surface of NiTi@Mg interpenetrating phase composites; (d) Boundary cracking between NiTi and Mg

phase composites after three-point bending test. The fracture surface of NiTi scaffolds shows a large number of micro-cracks (Fig. 6(a)) and dimples (Fig. 6(b)). The presence of dimples indicates that the NiTi scaffold has ductile fracture characteristics. However, these micro-cracks can act as initiation sites for fracture or preferred sites for crack propagation, leading to accelerated sample failure [26]. Similarly, dimples are found in the NiTi matrix of the NiTi@Mg interpenetrating phase composites, but the number of micro-cracks is significantly reduced compared to Fig. 6(a) (see Fig. 6(c)). Therefore, the infiltration of Mg alters the fracture mode of the NiTi scaffold, enhancing both fracture strength and plasticity. Moreover, cleavage planes and secondary cracks are present in the fractured regions of the Mg fillers, indicating typical transgranular fracture modes [27]. The propagation of secondary cracks is caused by the local stress variations during deformation. Additionally, visible cracks appear at the Mg and NiTi interface of the NiTi@Mg interpenetrating phase composites, which is largely due to stress transfer at the heterointerface [11].

Cross-sectional morphologies of the fractured sample (Fig. 7) were analyzed to investigate the crack initiation and propagation paths, revealing the presence of irregularly-shaped extended cracks and secondary cracks of the Mg filler and the interface cracks of NiTi/Mg near the fracture. The crack distribution of the cross-section indicates that the crack initiation of the NiTi@Mg interpenetrating phase composites takes place at the Mg filler and the NiTi/Mg interface, with secondary cracks or longer crack propagation paths consuming more energy during the fracture process [28]. The change in irreversible deformation energy (E_{consumed}) is shown in Fig. 5(d) to support this observation.

In order to gain deeper insights into the formation and propagation of cracks, transmission electron microscopy (TEM) samples of the deformed interfacial region were prepared using focused ion beam (FIB), as depicted in Figs. 8(a) and (b). A comparison of the microstructure in the deformed interfacial region with the undeformed area (Fig. 3(a)) revealed that the Mg filler exhibited numerous irregular dark regions, resulting from dislocation entanglement that led to the formation of high-density dislocations. This observation was made in the bright-field image of Fig. 8(c) at the

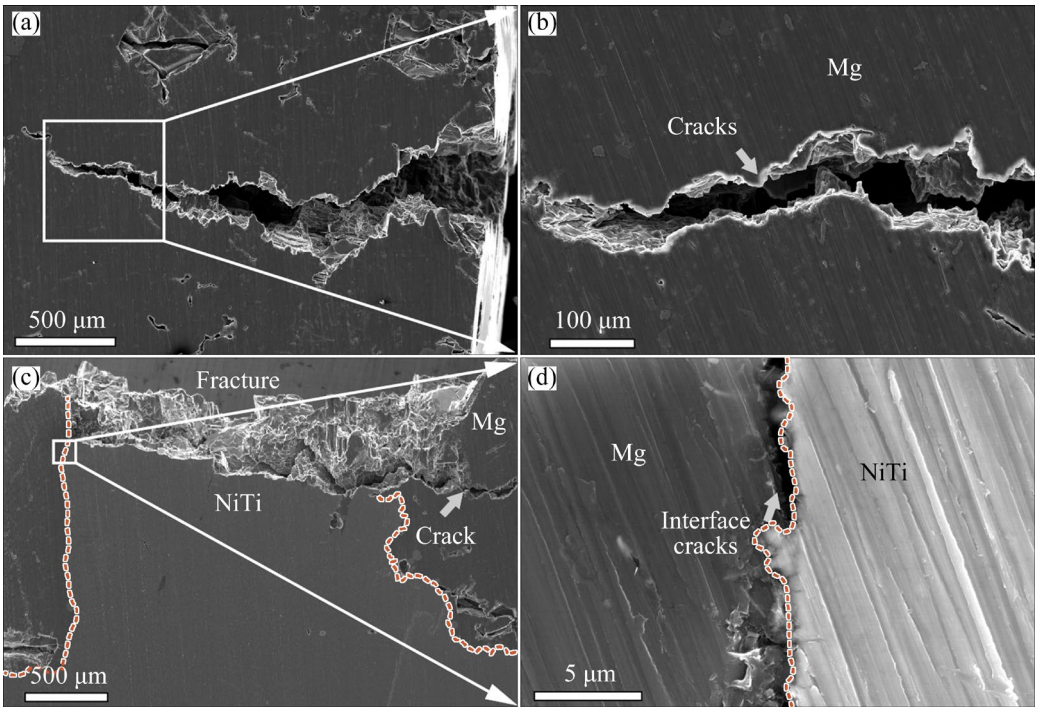

Fig. 7 SEM images of NiTi@Mg interpenetrating structure: (a) Crack propagation morphology in Mg filler; (b) Zoom-in image of boxed area in (a); (c) Crack distribution of fracture section; (d) Zoom-in image of boxed area in (c)

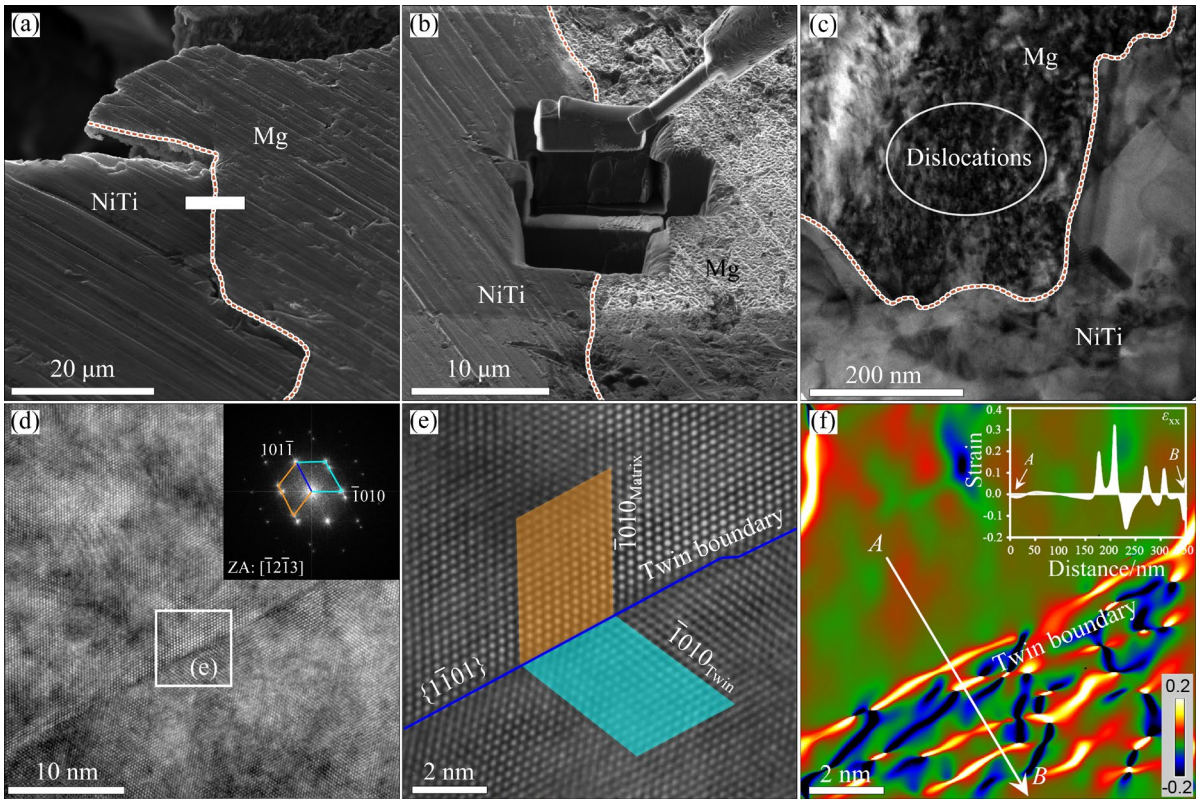

Fig. 8 Microstructures of deformed NiTi/Mg interface: (a) Fracture morphologies of NiTi@Mg interpenetrating phase composites; (b) NiTi/Mg interface sample obtained from (a) by FIB; (c) TEM image of NiTi/Mg interface at deformed region; (d) HRTEM image of Mg matrix and inset giving Fourier transform diffraction spectrum; (e) Interface as $\{1\bar{1}01\}$ compression twin plane; (f) Plots of strain components ε_{xx} obtained by GPA: $x_1//[1\bar{1}01]$, $x_2//[\bar{1}010]$ (The inset in (f) shows strain values in the A to B interval)

white circle-marked area. This finding suggests that the interface of the NiTi@Mg interpenetrating phase composites undergoes severe plastic deformation during deformation [7,15]. The dislocation source of the 3D interconnect interface is believed to have originated in the soft region of Mg. While the hard and adjacent soft zones undergo simultaneous deformation, the deformation primarily affects the Mg matrix of the soft zone [5]. This difference is thought to be due to the unequal dislocation transport in terms of slip direction and Burgers vector, resulting from the difference in the slip system [15]. The slip system of Mg alloys is generally limited, and dislocation accumulation within grains or at grain boundaries can be easily detected during plastic deformation [29]. To accommodate deformation during loading, the Mg filler is twinned, as depicted in Figs. 8(d) and (e). Mechanical twinning can increase the number of dislocations slip channels and reduce the effective slip distance, thus contributing to the occurrence of work hardening during deformation [30]. Additionally, the strain partitioning behavior at the mechanical twin interface was investigated using the gradient of the phase angle (GPA), which was calculated from the Fourier transform image in Fig. 8(e) by two non-collinear *g*-vectors. The strain distribution is depicted in Fig. 8(f), where high-density strain is observed at the twin interface and $(\bar{1}010)$ twins, with strain ranging from −0.16 to 0.32. Moreover, stress concentration of dislocation accumulation is also a critical consideration in Mg alloys during deformation [31].

3.4 Finite element modelling

In addition to evaluating the microscopic and local damage, this study also considers the macroscopic damage behavior of NiTi@Mg interpenetrating phase composites under stress. To this end, a three-dimensional nonlinear quasi-static finite element model is developed in Abaqus/Explicit to simulate three-point bending and compression experiments. This model combines the concept of attribute and damage theory and is capable of capturing the damage development process of the composites [1,15,32,33]. The mechanical properties of NiTi and Mg materials are modeled, as shown in Figs. 9 and 10.

The behavior of the NiTi@Mg interpenetrating phase composites under bending and compressive loads was analyzed using Von Mises stress distribution. Figure 9 presents the simulation results of the three-point bending test, where the maximum equivalent stress is observed in the middle area of the load concentration. Specifically, the hard NiTi scaffold bears a larger force during deformation resistance, with a maximum stress of approximately 600 MPa, while the soft Mg filler generates a certain back stress [16,21,23]. This behavior is similar to that of the “hard brick-and-soft mortar” structure, where a strong back-stress hardening effect occurs between the connected “brick” and “mortar” domains [16].

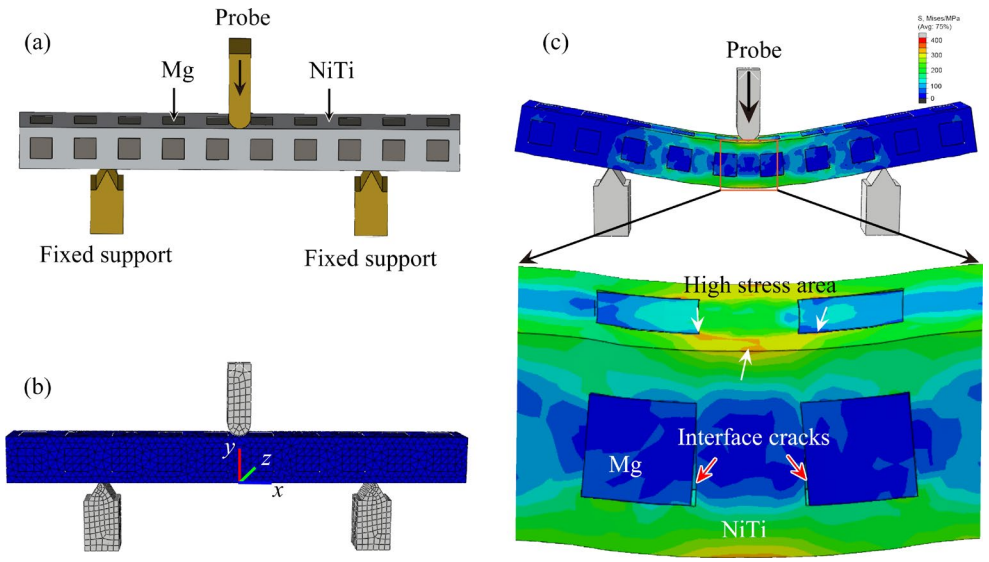

Fig. 9 Three-point bending simulation: (a) Geometric modeling of three-dimensional loading system; (b) Three-point bending finite element model; (c) Von Mises stress distribution

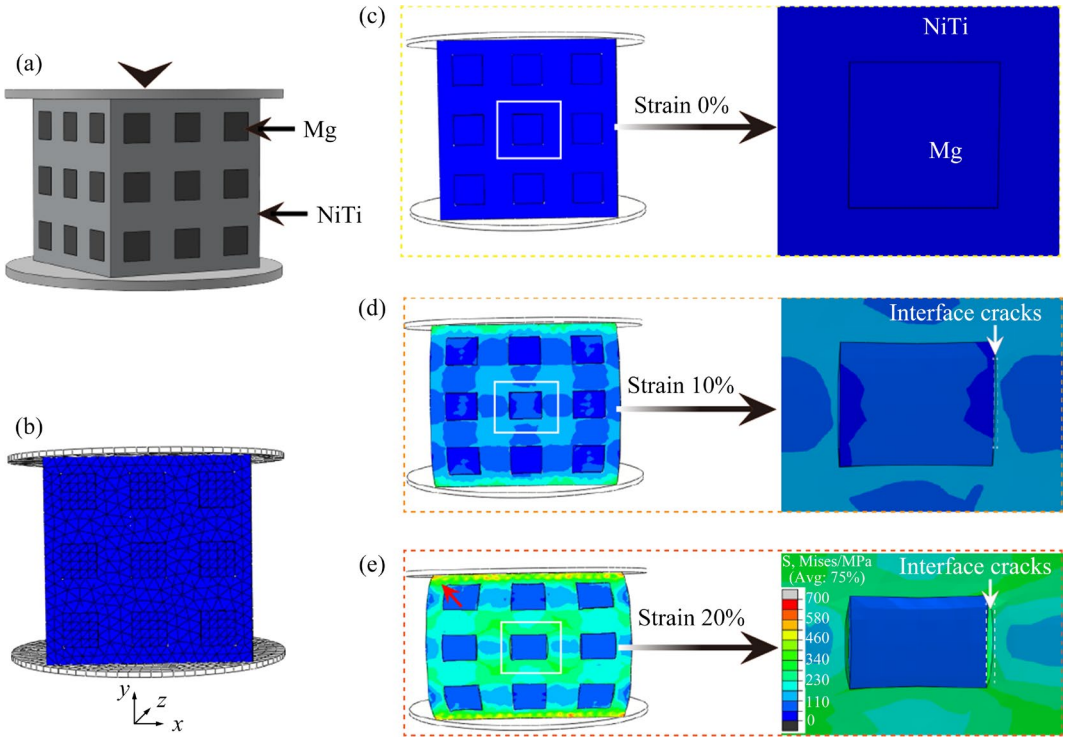

Fig. 10 NiTi@Mg composites structural compression simulation results: (a) Geometric modeling of three-dimensional loading system; (b) Compression finite element model; (c−e) Evolution of stress and interfacial crack over load history and final damage pattern

During bending and compression, cracks are observed at the interface of NiTi and Mg, as shown in Fig. 9(c) by the red arrows, which is consistent with the experimental results of fracture surface (Fig. 6) and cross section (Fig. 7). These interface cracks are attributed to the accumulation of dislocations at the interface during plastic deformation and stress concentration. When the stress exceeds the critical shear stress, subsequent crack initiation and propagation occur [16].

Figure 10 depicts the results of quasi-static compressive finite element simulation of NiTi@Mg interpenetrating phase composites. As shown in Figs. 10(c−e), the inhomogeneity of stress distribution in the NiTi@Mg model increases with the rise of loading. The stress concentration primarily occurs at the contact position between the NiTi support and anvil, which is indicated by the red arrow in Fig. 10(e). Generally, the failure of composite materials initiates the location with high stress concentration [15,33]. For instance, JEONG et al [15] demonstrated that the damage of FeCr/Mg composites takes place preferentially in the soft domain where the stress concentrates. Furthermore, it is noticeable that the cracks typically appear at the contact interface in the longitudinal direction of the soft and hard regions, and the cracks propagate further with increasing compression. Usually, the crack begins at the location with maximum tensile stress. Hence, the compression damage, d_C, can be described by Eq. (1), which is capable of capturing the development of compression fracture in the simulation process [34]:

$$d_C = 1 - \frac{\sigma_C}{\sigma_{CU}} \tag{1}$$

where σ_C is the compressive stress, and σ_{CU} is the compressive strength.

4 Discussion

4.1 Interface formation and strengthening mechanism

The interfacial bonding force is a crucial factor that determines the mechanical properties of composites [16]. Typically, the heterogeneous nature of composite materials leads to plastic incompatibility, resulting in the preferential formation of micro-cracks at the interface [5,8]. When the stress exceeds the interface bonding

strength, micro-cracks are formed at the interface, leading to material failure due to high stress concentration [16,33]. Therefore, to obtain composites with exceptional mechanical properties, 3D printing and metallurgical perfusion are combined to prepare metallurgically bonded Mg and NiTi interfaces, which has been demonstrated in earlier studies [5,15]. The macroscopic bonding is achieved by fully immersing splashed NiTi powders in the Mg filler, thereby enhancing the binding force between the magnesium fillers and the NiTi scaffolds (Fig. 2(b)). Microscopically, TEM analysis of the interface reveals that the two materials, Mg and NiTi, diffuse and form metallurgical bonds (Fig. 8). Notably, no apparent voids are found in the scaffold or filling area, indicating that Mg provides suitable conditions for atomic diffusion during casting, consistent with other composite materials prepared under different fabrication conditions [13]. These findings confirm that appropriate atomic diffusion and metallurgical bonding between heterogeneous materials are the primary reasons for the excellent mechanical properties of composites.

Strength and fracture toughness are two vital mechanical properties for structure materials, yet they often exhibit a mutually exclusive relationship with each other [6]. Composite strengthening is an effective approach to improve the properties of alloys, achieving high strength and ductility combinations through the synergistic contribution of different phases [10]. The interpenetrated structure obviously endows NiTi@Mg with higher strength and fracture energy compared to NiTi scaffolds (Figs. 4 and 5). The good fracture energy of NiTi@Mg composites primarily arises from the following three aspects: (1) The bicontinuous nature and interpenetration of NiTi and Mg in three-dimensional space allow for an effective stress transfer within and between each phase; the deformation and cracking of the weak Mg phase are limited, resulting in the retarded fracture of the entire composite. (2) Microcrack initiation and propagation are localized within the Mg matrix and at the interface between constituents in the NiTi and Mg composites. Cracks inevitably encounters to the NiTi scaffold during propagation (Figs. 7 and 11), and the NiTi matrix can release strain energy through stress-induced martensitic transformation, thus avoiding premature fracture caused by the accumulate of dislocations [18,19]. Additionally, it can direct the growing crack to deflect and twist, promoting an increase in strength and toughness [6]. (3) The formation of deformation twins (DTs) in the Mg matrix involves a highly correlated inelastic shearing process, wherein adjacent atomic planes slip in the same way compared with ordinary dislocation plasticity [20]. This process absorbs elastic strain energy and delays the rapid expansion of shear bands and the generation of microcracks, thereby improving ductility.

Furthermore, the enhanced strength of the NiTi@Mg composites can be discussed by two aspects: heterostructure strengthening and deformation twins strengthening.

(1) Heterostructure strengthening mechanism

In fact, in the NiTi@Mg interpenetrating composites, the difference in physical properties between NiTi scaffolds and Mg fillers makes the stress and strain field distribution different in various parts of the composites. Taking NiTi@Mg as an example, the density of NiTi (6.5 g/cm^3) is about three times greater than that of Mg (1.7 g/cm^3), and the elastic modulus and Poisson ratio are also different either. Therefore, Fig. 9(c) and Fig. 10(e) show that the NiTi scaffolds suffer higher stress under high load, followed by NiTi/Mg interface and Mg matrix. However, non-uniform deformation of the NiTi scaffold (hard region) and Mg filler (soft region) leads to the production of positive stress in the hard zone and back stress in the soft zone, resulting in a heterogeneous deformation strengthening effect [15]. This effect enhances the yield strength and work hardening rates while maintaining inherent ductility [21,23], as evidenced by the significant dislocation accumulation in the Mg filler at the deformed interface (Fig. 8). Additionally, the mutual permeability and interconnectivity of Mg and NiTi compositions and structures in three-dimensional space facilitate stress transfer between each phase and mutual restraint during deformation. For instance, during crack propagation, Mg fillers are impeded by the NiTi strengthened phase interface, delaying the fracture of composite structural materials [6]. This observation supports the notion of heterogeneous deformation strengthening due to the constraints of adjacent soft/hard regions during deformation [5,15]. Consequently, the strength of the NiTi@Mg composites is enhanced by the mutual strengthening

of the microstructures with different characteristics during the deformation process [15,35].

(2) Twin strengthening mechanism

One of the key factors contributing to the enhanced strength of interpenetrating hetero-structured composites such as NiTi@Mg is the occurrence of deformation twinning within the Mg filler. The formation of mechanical twins, labeled as $\{1\bar{1}01\}$ twin systems by inverse fast Fourier transform (IFFT), as observed in Figs. 8(d) and (e) confirms this phenomenon. Deformation twinning is a common mode of plastic deformation for materials with hexagonal close-packed (HCP) structures, such as Mg alloys, due to the limited slip system [29]. It has been shown to be a prevalent mode of plastic deformation, especially when the slip mechanism is impeded [36]. Additionally, twin interfaces can enhance mechanical properties by interacting with dislocations and exhibiting greater mechanical stability compared to conventional grain boundaries [37]. As such, twinning strengthening is considered one of the primary reasons for the improved strength observed in NiTi@Mg interpenetrating phase composites.

4.2 Damaging process and mechanism

NiTi@Mg interpenetrating phase composites exhibit significantly improved mechanical properties compared to NiTi scaffolds. In the elastic stage (Stage I), there is no apparent plastic deformation at the interface of NiTi@Mg composites, but the soft zone undergoes high strain and dislocations slip and accumulate at the NiTi/Mg interface, generating back stress in the soft zone (Fig. 8(c)). This is the main factor responsible for the high yield strength of composite structural materials [21]. As deformation progresses, elastic deformation transforms into plastic deformation (Stage II). The NiTi hard region hinders dislocation transfer in the Mg soft region, and a large number of dislocations accumulate near the interface between the NiTi hard region and the Mg soft region [21,23]. Consequently, Mg at the NiTi/Mg interface region undergoes severe deformation, leading to the formation of cracks at the interface and a weakening of the coordinated deformation ability of the interface, as observed in the fractured SEM images (Figs. 6 and 7). This can be attributed to an interface detachment mechanism. However, in the soft region observed using TEM, Mg can undergo coordinated deformation through the mechanical twinning (Fig. 8), which mitigates the initiation and propagation of cracks to some extent [38]. As a result, cracks at this stage exist in the form of micro-cracks, which gradually expand to macro-cracks with increasing load (Fig. 7(d)). When the loading force reaches its peak, macroscopic cracks propagate rapidly, breaking the continuity of the sample structure (Stage III) [39]. The fracture process of NiTi@Mg interpenetrating phase composites is illustrated in Fig. 11. The damage process of composite materials under stress is constantly evolving, and the evolution process can be defined according to damage criterion (d) [40]:

$$d=\frac{\delta_{\mathrm{eq}}^{\mathrm{f}}(\delta_{\mathrm{eq}}-\delta_{\mathrm{eq}}^{\mathrm{f}})}{\delta_{\mathrm{eq}}(\delta_{\mathrm{eq}}^{\mathrm{f}}-\delta_{\mathrm{eq}}^{0})} \tag{2}$$

where δ_{eq} is the equivalent strain, δ_{eq}^{0} is the initial equivalent displacement, and $\delta_{\mathrm{eq}}^{\mathrm{f}}$ is the displacement at which the material is completely damaged.

The stress distribution and the location where cracks tend to form during the damage process can be detected through finite element simulations. It is

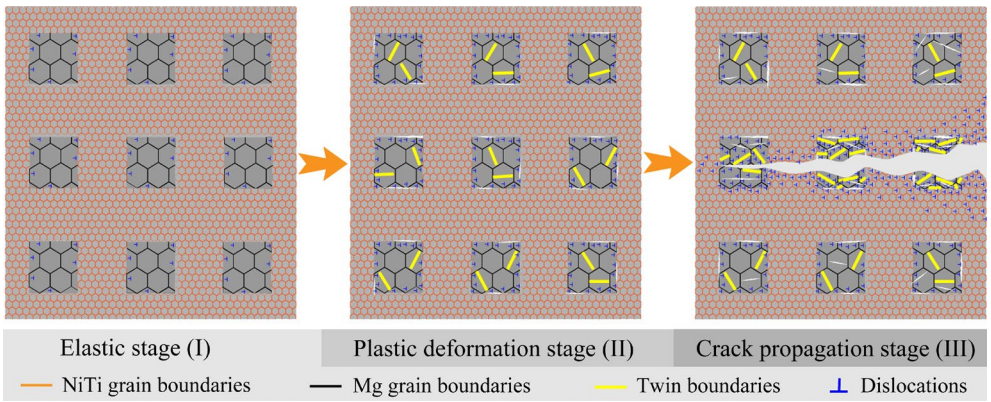

Fig. 11 Fracture mechanism of NiTi@Mg interpenetrating phase composites

commonly believed that the region of crack formation and stress concentration correspond with each other [32]. Bending simulations have also revealed that stress is concentrated near the loading position and occurs perpendicular to the loading direction on the beam. This is attributed to the fact that stress concentration often occurs in the beam position of the loading area, as depicted in Fig. 9(c). Experimental evidence in Fig. 7 has shown that this stress concentration leads to the formation of cracks. These findings are consistent with the discovery by LOSCH et al [41] that cracks tend to form in regions of high strain concentration which were identified by digital volume correlation analysis during compression of CrMnNi−Mg composites. As a result, the heterogeneous deformation between soft and hard zones in NiTi@Mg interpenetrating phase composites leads to mechanical incompatibility during deformation [14]. The deformation of Mg and NiTi occurs simultaneously, which creates a stress gradient near the interface to coordinate the differentiated strain, as shown in Figs. 9 and 10. These characteristics provide further evidence that interpenetrating composites offer greater reinforcement than scaffolds.

5 Conclusions

(1) A 3D interconnected NiTi@Mg composite was synthesized by combining 3D printing with infiltration, realizing the mutual diffusion of components to form a metallurgically bonded NiTi/Mg interface.

(2) The Mg filler plays a crucial role in promoting the lightweight design and strengthening effect of the interpenetrating phase composites, while facilitating effective load transfer and achieving high-energy absorption efficiency.

(3) The measured bending strength of the NiTi@Mg interpenetrating phase composite is 432 MPa, which is 2.5 times higher than that of the NiTi scaffold. The high compressive strength is attributed to the interpenetrating morphology and the strong back stress effect in the soft/hard regions.

(4) During the deformation process of the NiTi@Mg interpenetrating phase composites, mechanical incompatibility arises due to the heterogeneous deformation between the soft and hard regions, leading to preferential dislocation plugging and crack initiation in the soft Mg region. This observation is consistent with the numerical analysis results obtained for bending and compression.

CRediT authorship contribution statement

Yu-jing LIU: Conceptualization, Investigation, Writing – Review & editing; **Xiao-chun LIU:** Conceptualization, Formal analysis, Methodology, Resources; **Kun-mao LI:** Conceptualization, Investigation, Formal analysis, Writing – Original draft; **Xiang WU:** Investigation, Data curation; **Sheng-feng ZHOU:** Conceptualization, Methodology, Writing – Review & editing, Supervision; **Wei LI:** Resources; **Wen-cai ZHANG:** Investigation, Data curation.

Declaration of competing interest

The authors declare that they have no known competing financial interests or personal relationships that could have appeared to influence the work reported in this paper.

Acknowledgments

This work was supported by the National Natural Science Foundation of China (Nos. 52001030, 51803200, 52105356, 52003104), the Natural Science Foundation of Hunan Province, China (Nos. 2021JJ40590, 2021JJ40600), the Natural Science Foundation of Hunan Province Youth Fund, China (No. 2021JJ20011), the Major Research Plan of the National Natural Science Foundation of China (No. 92166112), the Project of MOE Key Lab of Disaster Forecast and Control in Engineering in Jinan University, China (No. 20200904006), the Guangdong Province Basic and Applied Basic Research Foundation, China (No. 2020B1515420004), the Guangxi Key Laboratory of Information Materials, China (No. 211003-K), the Open Project Program of the State Key Laboratory of Mechanical Transmissions in Chongqing University, China (No. SKLMT-MSKFKT-202102), and the Fundamental Research Funds for the Central Universities, China (No. 21622110).

References

[1] ZHANG Yun-fei, HSIEH M T, VALDEVIT L. Mechanical performance of 3D printed interpenetrating phase composites with spinodal topologies [J]. Composite Structures, 2021, 263: 113693.

[2] HUANG C X, WANG Y F, MA X L, YIN S, HÖPPEL H W, GÖKEN M, WU X L, GAO H J, ZHU Y T. Interface affected zone for optimal strength and ductility in heterogeneous laminate [J]. Materials Today, 2018, 21(7): 713−719.

[3] MA Xu, SUN Hao-dong, KOU Si-jie, FAN Shang-wu, DENG Juan-li, ZHANG Li-tong, CHENG Lai-fei. Flexural strength and wear resistance of C/C−SiC brake materials

improved by introducing SiC ceramics into carbon fiber bundles [J]. Ceramics International, 2021, 47(17): 24130−24138.

[4] XIE Ke-wei, NIE Jin-feng, HU Kai-qi, MA Xia, LIU Xiang-fa. Improvement of high-temperature strength of 6061 Al matrix composite reinforced by dual-phased nano-AlN and submicron-Al_2O_3 particles [J]. Transactions of Nonferrous Metals Society of China, 2022, 32(10): 3197−3211.

[5] ZHANG Ming-yang, YU Qin, LIU Zeng-qian, ZHANG Jian, TAN Guo-qi, JIAO Da, ZHU Wen-jun, LI Shu-jun, ZHANG Zhe-feng, YANG Rui, RITCHIE R O. 3D printed Mg-NiTi interpenetrating-phase composites with high strength, damping capacity, and energy absorption efficiency [J]. Science Advances, 2020, 6: eaba5581.

[6] ZHANG Ming-yang, ZHAO Ning, YU Qin, LIU Zeng-qian, QU Rui-tao, ZHANG Jian, LI Shu-jun, REN De-chun, BERTO F, ZHANG Zhe-feng, RITCHIE R O. On the damage tolerance of 3-D printed Mg−Ti interpenetrating-phase composites with bioinspired architectures [J]. Nature Communications, 2022, 13: 3247.

[7] GAO W J, ZHANG W W, ZHANG T, YANG C, HUANG X S, LIU Z Y, WANG Z, LI W H, LI W R, LI L, LIU L H. Large tensile plasticity in Zr-based metallic glass/stainless steel interpenetrating-phase composites prepared by high pressure die casting[J]. Composites Part B, 2021, 224: 109226.

[8] ZHOU Zhao-yao, YAO Bi-bo, DUAN Liu-yang, QIN Jie. Production and anisotropic compressibility of 304 stainless steel fiber/ZA8 zinc alloy interpenetrating phase composites [J]. Journal of Alloys and Compounds, 2017, 727: 146−152.

[9] STERNITZKE M, KNECHTEL M, HOFFMAN M, BROSZEIT E, RÖDEL J. Wear properties of alumina/ aluminum composites with interpenetrating networks [J]. Journal of the American Ceramic Society, 1996, 79(1): 121−128.

[10] RAZZAGHI M, KASIRI A M, BAKHSHESHI R H R, GHAYOUR H. Microstructure, mechanical properties, and in-vitro biocompatibility of nano-NiTi reinforced Mg−3Zn−0.5Ag alloy: Prepared by mechanical alloying for implant applications [J]. Composites Part B, 2020, 190: 107947.

[11] CAO Meng-xin, JIANG Feng-chun, ZHOU Rui, QIN Ruo-nan, ZHANG He-xin, WANG Zhen-qiang, GUO Chun-huan. A novel bio-inspired metal hollow sphere filled TC4/Al sandwich composite: Fabrication and compressive properties [J]. Materials Today Communications, 2022, 31: 103349.

[12] LIU Pei, WANG Ai-qin, XIE Jing-pei, HAO Shi-ming. Characterization and evaluation of interface in SiC_p/2024 Al composite [J]. Transactions of Nonferrous Metals Society of China, 2015, 25(5): 1410−1418.

[13] SHAYANPOOR A A, REZAEI A H R. Microstructural and mechanical investigations of powder reinforced interface layer of hot extruded Al/Cu bimetallic composite rods [J]. Journal of Manufacturing Processes, 2022, 77: 313−328.

[14] LI Dong-hai, WANG Bin-bin, LUO Liang-shun, LI Xue-wen, XU Yan-jin, LI Bin-qiang, WANG Liang, LIU Wen-yi, HAN Bao-shuai, SU Yan-qing, GUO Jing-jie, FU Heng-zhi. The interface structure and its impact on the mechanical behavior of TiAl/Ti_2AlNb laminated composites [J]. Materials Science and Engineering A, 2021, 827: 142095.

[15] JEONG Y B, WADA T, JOO S-H, PARK J-M, MOON J, KIM H S, OKULOV I V, PARK S H, LEE J H, KIM K B, KATO H. Beyond strength-ductility trade-off: 3D interconnected heterostructured composites by liquid metal dealloying [J]. Composites Part B, 2021, 225: 109266.

[16] LIU Xiao-chun, LIU Zheng, LIU Yu-jing, ZAFAR Z, LU Yan-jin, WU Xiang, JIANG Yue, XU Zhi-guang, GOU Zheng-hua, LI Shu-jun. Achieving high strength and toughness by engineering 3D artificial nacre-like structures in Ti6Al4V-Ti metallic composite[J]. Composites Part B, 2022, 230: 109552.

[17] CHO K, RAJAN, G, FARRAR P, PRENTICE L, PRUSTY B G. Dental resin composites: A review on materials to product realizations [J]. Composites Part B, 2022, 230: 109495.

[18] ZHANG Yin-tao, LIU Jia, WANG Li-qiang, WEI Dai-xiu, LIU Chang-xi, WANG Kuai-she, TANG Yu-jin, ZHANG Ling, LU Wei-jie. Porous NiTiNb alloys with superior strength and ductility induced by modulating eutectic microregion [J]. Acta Materialia, 2022, 239: 118295.

[19] LV Yu-ting, LIU Guo-hao, WANG Bing-hao, TANG Yu-jin, LIN Zheng-jie, LIU Jia, WEI Gui-jiang, WANG Li-qiang. Pore strategy design of a novel NiTi−Nb biomedical porous scaffold based on a triply periodic minimal surface [J]. Frontiers in Bioengineering and Biotechnology, 2022, 10: 910475.

[20] ZHU Hong-mei, LUO Cheng-ping, LIU Jiang-wen, JIAO Dong-ling. Growth twinning behavior of cast Mg−Zn−Cu−Zr alloys [J]. Transactions of Nonferrous Metals Society of China, 2014, 24(2): 316−320.

[21] ZHU Yun-tian, AMEYAMA K, ANDERSON P M, BEYERLEIN I J, GAO Hua-jian, KIM H S, LAVERNIA E, MATHAUDHU S, MUGHRABI H, RITCHIE R O, TSUJI N, ZHANG Xiang-yi, WU Xiao-lei. Heterostructured materials: Superior properties from hetero-zone interaction [J]. Materials Research Letters, 2021, 9: 1−31.

[22] WANG Jun, FERDOWSI M R G, KADA S R, LYNCH P A, WANG Zhi-yang, KIMPTON J A, BARNETT M R. Stress relaxations during cyclic loading-unloading in precipitation hardened Mg−4.5Zn [J]. Acta Materialia, 2021, 205: 116531.

[23] YANG Mu-xin, PAN Yue, YUAN Fu-ping, ZHU Yun-tian, WU Xiao-lei. Back stress strengthening and strain hardening in gradient structure [J]. Materials Research Letters, 2016, 4: 145−151.

[24] HU Ke, LE Qi-chi, ZHOU Wei-yang, LI Chun-yu, LIAO Qi-yu, YU Fu-xiao. Three-point bending behavior and microstructural evolution of ZM20E, ZM20EX and AZ31 tubes [J]. Materials Characterization, 2020, 159: 110065.

[25] LAI Tao, XU Ji-lin, XIAO Qi-fei, TONG Yun-xiang, HUANG Jun, ZHANG Jian-ping, LUO Jun-ming, LIU Yong. Preparation and characterization of porous NiTi alloys synthesized by microwave sintering using Mg space holder [J]. Transactions of Nonferrous Metals Society of China, 2021, 31: 485−498.

[26] LI Bin-qiang, WANG Liang, WANG Bin-bin, LI Dong-hai, CUI Ran, SU Bao-xian, YAO Long-hui, LUO Liang-shun, CHEN Rui-run, SU Yan-qiang, GUO Jing-jie, FU Heng-zhi. Solidification characterization and its correlation with the mechanical properties and functional response of NiTi shape memory alloy manufactured by electron beam freeform fabrication [J]. Additive Manufacturing, 2021, 48: 102468.

[27] LIU Wen-cai, JIANG Long-kang, CAO Liang, MEI Jun, WU

Guo-hua, ZHANG Song, XIAO Lv, WANG Shao-hua, DING Wen-jiang. Fatigue behavior and plane-strain fracture toughness of sand-cast Mg−10Gd−3Y−0.5Zr magnesium alloy [J]. Materials & Design, 2014, 59: 466−474.

[28] YE Xian-wei, WAN Ming-pan, HUANG Chao-wen, LEI Min, JIAN Shi-chao, ZHANG Yuan, XU Dan, HUANG Fang. Effect of aging temperature on mechanical properties of TC21 alloy with multi-level lamellar microstructure [J]. Materials Science and Engineering A, 2022, 840: 142825.

[29] WANG Tao, YANG Lun, TANG Zhao-feng, WU Lei, YAN Huan-yuan, LIU Chao, MA Yun-zhu, LIU Wen-sheng, YU Zhao-ji. Microstructure, mechanical properties and deformation mechanism of powder metallurgy AZ31 magnesium alloy during rolling [J]. Materials Science and Engineering A, 2022, 844: 143042.

[30] LI Kun-mao, YANG Jun-jie, YI Yan-liang, LIU Xiao-chun, LIU Yu-jing, ZHANG Lai-chang, ZHANG Wen-cai, LI Wei, CHEN Dong-chu, ZHOU Sheng-feng. Enhanced strength-ductility synergy and mechanisms of heterostructured Ti6Al4V−Cu alloys produced by laser powder bed fusion [J]. Acta Materialia, 2023, 256: 119112.

[31] ZHANG Xue-jian, WANG Hong-wei, YE Feng-bai, ZOU Chun-ming, WEI Zun-jie. Cooperative effect of Mg and Si contents on the microstructural evolution, mechanical performance, and deformation behavior of cast Al−Li−Mg−Si alloys [J]. Materials Science and Engineering A, 2022, 841: 142976.

[32] SCHUKRAFT J, HORNY D, SCHULZ K, WEIDENMANN K A. 3D modeling and experimental investigation on the damage behavior of an interpenetrating metal ceramic composite (IMCC) under compression [J]. Materials Science and Engineering A, 2022, 844: 143147.

[33] GHAYOOR H, HOA S V, MARSDEN C C. A micromechanical study of stress concentrations in composites [J]. Composites Part B, 2018, 132: 115−124.

[34] NGUYEN V V, CHOUDHRY N K, PANDA B, NGUYEN X H, TRAN P. Performance of concrete beam reinforced with 3D printed Bioinspired primitive scaffold subjected to three-point bending [J]. Automation in Construction, 2022, 134: 104060.

[35] LIU Qing, QI Fu-gong, DING Hai-min, FAN Xiao-liang, YUE Ying. Distribution of stress and strain between adjacent particles in particulate reinforced metal matrix composites [J]. Transactions of Nonferrous Metals Society of China, 2018, 28(11): 2314−2323.

[36] AHMADI M, SALGIN B, KOOI B J, PEI Y T. The effect of grain refinement on the deformation and cracking resistance in Zn−Al−Mg coatings [J]. Materials Science and Engineering A, 2022, 840: 142995.

[37] FU Hui, GE Bin-cheng, XIN Yun-chang, WU Rui-zhi, FERNANDEZ C, HUANG Jian-yu, PENG Qiu-ming. Achieving high strength and ductility in magnesium alloys via densely hierarchical double contraction nanotwins [J]. Nano Letters, 2017, 17: 6117−6124.

[38] CUI Xiao-ming, YU Zhi-lei, LIU Fei, DU Zhao-xin, BAI Pu-cun. Influence of secondary phases on crack initiation and propagation during fracture process of as-cast Mg−Al−Zn−Nd alloy [J]. Materials Science and Engineering A, 2019, 759: 708−714.

[39] QIN Xiao-feng, SU Hai-jian, FENG Yu-jie, ZHAO Hong-hui, PHAM T N. Fracture and deformation behaviors of saturated and dried single-edge notched beam sandstones under three-point bending based on DIC [J]. Theoretical and Applied Fracture Mechanics, 2022, 117: 103204.

[40] TUO Hong-liang, LU Zhi-xian, MA Xiao-ping, ZHANG Chao, CHEN Shu-wen. An experimental and numerical investigation on low-velocity impact damage and compression-after-impact behavior of composite laminates [J]. Composites Part B, 2019, 167: 329−341.

[41] LOSCH K, SCHLADITZ K, BALLASCHK U, BEREK H, ANEZIRIS C G. Interrupted in-situ compressive deformation experiments on MMC foams in an XCT: Experiments and estimation of displacement fields [J]. Image Analysis & Stereology, 2014, 33: 131−145.

具有优异弯曲性能的轻质 3D 互穿 NiTi@Mg 复合材料的制备

刘玉敬[1]，刘小春[1]，李坤茂[2]，吴 翔[1]，周圣丰[2,3]，李 卫[2]，张文财[4]

1. 长沙理工大学 材料科学与工程学院 金属研究所，长沙 410004；
2. 暨南大学 先进耐磨蚀及功能材料研究院，广州 510632；
3. 重庆大学 机械传动国家重点实验室，重庆 400044；
4. 暨南大学 附属第一医院 骨科，广州 510632

摘 要：采用增材制造(AM)与熔渗技术相结合，开发一种新型高强轻质互穿相复合材料 NiTi@Mg，并对 NiTi@Mg 复合材料的界面结合、三点弯曲和循环强化性能进行研究。结果表明，在 NiTi−Mg 界面处形成了冶金结合界面。与 NiTi 支架相比，NiTi@Mg 互穿相复合材料的弯曲强度提高了 2.5 倍，压缩强度提高了 1.7 倍。在弯曲过程中，观察到大量位错堆积在界面处的软 Mg 区域。此外，有限元模型显示，弯曲过程中裂纹萌生的应力集中区位于 NiTi 与 Mg 的界面处。NiTi@Mg 复合材料的强化机制归因于 Mg 的孪生强化和异质结构强化。

关键词：金属复合材料；NiTi @ Mg；弯曲性能；有限元模拟；强化机制

(Edited by Xiang-qun LI)